REPORT DOCUMENTATION PAGE

Form Approved OMB NO. 0704-0188

1. REPORT DATE (DD-MM-YYYY)	2. REPORT TYPE	3. DATES COVERED (From - To)
25-08-2009	Final Report	1-Sep-2002 - 31-Aug-2007

4. TITLE AND SUBTITLE
Mechanisms of Aging of Phosphylated Serine Hydrolases: Final Report

5a. CONTRACT NUMBER
DAAD19-02-1-0388

5b. GRANT NUMBER

5c. PROGRAM ELEMENT NUMBER

6. AUTHORS
Rudy J. Richardson, Sanjeeva J. Wijeyesakere

5d. PROJECT NUMBER

5e. TASK NUMBER
611102

5f. WORK UNIT NUMBER

7. PERFORMING ORGANIZATION NAMES AND ADDRESSES
University of Michigan - Ann Arbor
Room 1058 Wolverine Tower
3003 South State Street
Ann Arbor, MI 48109 -1274

8. PERFORMING ORGANIZATION REPORT NUMBER

9. SPONSORING/MONITORING AGENCY NAME(S) AND ADDRESS(ES)
U.S. Army Research Office
P.O. Box 12211
Research Triangle Park, NC 27709-2211

10. SPONSOR/MONITOR'S ACRONYM(S)
ARO

11. SPONSOR/MONITOR'S REPORT NUMBER(S)
44379-LS.21

12. DISTRIBUTION AVAILIBILITY STATEMENT
Approved for public release; Distribution Unlimited

13. SUPPLEMENTARY NOTES
The views, opinions and/or findings contained in this report are those of the author(s) and should not contrued as an official Department of the Army position, policy or decision, unless so designated by other documentation.

14. ABSTRACT
The overall goal was to study mechanisms of aging of serine esterases inhibited by organophosphorus compounds capable of producing acute and delayed neurotoxicity. Acetylcholinesterase (AChE), butyrylcholinesterase (BChE), and neuropathy target esterase catalytic domain (NEST) were reacted with diisopropylphosphorofluoridate (DFP) and N,N'-diisopropylphosphorodiamidofluoridate (mipafox, MIP). Bimolecular rate constants of inhibition and first-order rate constants of aging were determined colorimetrically. Phosphyl adducts of inhibited and aged

15. SUBJECT TERMS
acetylcholinesterase (AChE), aging reaction, biomarker, biosensor, butyrylcholinesterase (BChE), DFP, inhibition, kinetics, mass spectrometry, mipafox, neuropathy target esterase (NTE), NTE catalytic domain (NEST), neurotoxicity, organophosphorus

16. SECURITY CLASSIFICATION OF:			17. LIMITATION OF ABSTRACT	15. NUMBER OF PAGES	19a. NAME OF RESPONSIBLE PERSON
a. REPORT	b. ABSTRACT	c. THIS PAGE			Rudy Richardson
U	U	U	SAR		19b. TELEPHONE NUMBER 734-936-0769

ARO FINAL REPORT: Narrative Section
Proposal Number: 44379-LS
Agreement Number: DAAD19-02-1-0388
PI: Rudy J. Richardson, ScD, DABT
Report Authors: Rudy J. Richardson and Sanjeeva J. Wijeyesakere

TABLE OF CONTENTS

2. List of Tables and Figures

List of Tables

List of Figures

3. Statement of the Problem Studied

3.1. Overall goal.

The overall goal of the research project was to use kinetics, mass spectrometry, and computational modeling to investigate mechanisms of aging of serine hydrolases inhibited by organophosphorus (OP) compounds.

3.2. Objectives.

The objectives of the research were to test the following main hypotheses that were based on considerable literature background and preliminary data:

3.2.1. Acetylcholinesterase (AChE), butyrylcholinesterase (BChE), and neuropathy target esterase (NTE) catalytic domain (NEST) inhibited by diisopropylphosphorofluoridate (DFP) undergo postinhibitory reactions (e.g., aging) to yield monoisopropylphosphyl adducts on their active site serines.

3.2.2. AChE and BChE inhibited by *N*,*N*′-diisopropylphosphorodiamidofluoridate (mipafox, MIP), a water-soluble analogue of DFP, likewise undergo aging to yield monoisopropylphosphyl adducts on their active site serines.

3.2.3. In contrast, NEST inhibited by MIP does not undergo a similar postinhibitory reaction and retains a diisopropylphosphyl adduct on its active site serine, in which case aging proceeds by reversible deprotonation.

3.2.4. Computational modeling may be used to gain insight into known interactions of OP compounds with serine hydrolases and to make predictions about currently unknown interactions of existing or new compounds with existing or new macromolecular targets.

4.3. Specific aims.

The hypotheses were tested and additional relevant data were generated by carrying out the following specific aims:

4.3.1. *Kinetics*. Bimolecular rate constants of inhibition (k_i) and the first-order rate constants of aging (k_4) were determined for human recombinant AChE, horse serum BChE, and human recombinant NEST inhibited by DFP and MIP. Inhibitory and postinhibitory kinetics studies were needed to fill gaps in the existing database and especially to confirm preliminary observations that the results of postinhibitory kinetics of MIP-inhibited NEST were not consistent with a conventional aging mechanism.

4.3.2. *Mass spectrometry*. Adducts on the active site serines of AChE, BChE, and NEST inactivated with DFP or MIP were determined, allowing sufficient time for aging or other postinhibitory reactions to occur as determined from the kinetics studies in Aim (1) above. Peptide mass mapping with surface-enhanced laser desorption/ionization time-of-flight mass spectrometry (SELDI-TOF-MS) was used to identify adducts.

4.3.3. *Computational molecular modeling*. Computational investigations were carried out, focusing on developing a homology model of NEST, given that tertiary structures of AChE and BChE were already known, but that the tertiary structure of NTE and NEST were unknown.

5. Summary of the Most Important Results

5.1. *Kinetics*. Rate constants for inhibitory and postinhibitory reactions of DFP and MIP with serine esterases are summarized below for AChE (Table 1), BChE (Table 2), and NEST (Table 3):

Table 1. Kinetic constants for inhibition and aging of AChE by DFP or MIP [a,b]

Inhibitor	k_i ($M^{-1}min^{-1}$)	k_4 (min^{-1})
DFP	$(1.72 \pm 0.07) \times 10^6$	$(2.13 \pm 0.16) \times 10^{-2}$
MIP	$(1.47 \pm 0.07) \times 10^4$	$(1.92 \pm 0.13) \times 10^{-2}$

[a] Data from Kropp and Richardson (2006).
[b] Values are means ± SEM (n = 4 experiments).

Table 2. Kinetic constants for inhibition and aging of BChE by DFP or MIP [a,b]

Inhibitor	k_i ($M^{-1}min^{-1}$)	k_4 (min^{-1})
DFP	$(1.83 \pm 0.18) \times 10^6$	$(8.49 \pm 0.99) \times 10^{-3}$
MIP	$(1.28 \pm 0.05) \times 10^6$	$(1.21 \pm 0.28) \times 10^{-2}$

[a] Data from Kropp and Richardson (2007).
[b] Values are means ± SEM (n = 4 experiments)

Table 3. Kinetic constants for inhibition and aging of NEST by DFP or MIP [a,b]

Inhibitor	k_i ($M^{-1}min^{-1}$)	k_4 (min^{-1})	
	pH 8.0	pH 8.0	pH 5.2
DFP	$(1.72 \pm 0.0180) \times 10^4$	$(1.08 \pm 0.41) \times 10^{-1}$	$(1.81 \pm 0.34) \times 10^{-1}$
MIP	$(1.88 \pm 0.061) \times 10^3$	*c*	*d*

[a] Data from Kropp *et al*. (2004).
[b] Values are means ± SEM (n = 4 experiments).
[c] No activity was restored for all time points (0–18 h).
[d] Activity was completely restored for all time points.

DFP was over 100-fold more potent than MIP as an inhibitor of AChE and about 9-fold more potent than MIP against NEST, whereas these inhibitors were approximately equipotent against BChE.

Rates of aging of AChE inhibited by DFP or MIP were approximately equal, with half-times of about 32.5 min and 36.1 min, respectively. Similarly, rates of aging of BChE inhibited by DFP or MIP were comparable, with half-times of 81.3 min and 57.3 min, respectively. NEST inhibited with DFP aged

relatively rapidly at pH 8.0 or pH 5.2 with half-times of 6.41 and 3.83 min, respectively. NEST inhibited with MIP appeared to age instantaneously at pH 8.0 and no activity could be restored during 0 to 18 h, whereas at pH 5.2 no aging took place and all activity could be restored for all time points. Thus, aging of MIP-inhibited NEST was pH-dependent and the results were consistent with aging involving deprotonation of a phosphoroamido nitrogen.

5.2. *Mass spectrometry*. Average masses of intact (nonaged) and kinetically aged adducts on the active site peptides of serine hydrolases reacted with DFP or MIP are shown for AChE (Table 4) BChE (Table 5) and NEST (Table 6).

Table 4. Differences in average mass of MH^+ ions of active site peptides from intact or aged adducts of AChE with DFP or MIP [a,b]

Data type	Δ*m* DFP intact	Δ*m* DFP aged	Δ*m* MIP intact	Δ*m* MIP singly aged	Δ*m* MIP doubly aged
Observed	165.0 ± 0.9	123.8 ± 0.7	163.4 ± 1.0	ND[c]	80.7 ± 0.9[d]
Theoretical	164.1	122.1	162.2	121.1	80.0

[a] Data from Kropp and Richardson (2006).

[b] Values are means ± SEM ($n \geq 4$ experiments). The *m/z* values (average mass) for the MH^+ ion of the unreacted tryptic digest peptide containing the active site Ser are 4270.8 ± 0.3 (observed) and 4270.8 (theoretical). Theoretical values of Δ*m* (*m/z*) take into account the average mass of the Ser hydroxyl proton that is lost in the organophosphorylation reaction. Theoretical nonaged (intact) adducts for DFP and MIP are diisopropylphosphoryl and *N,N′*-diisopropylphosphoroamidoyl, respectively. Theoretical aged adducts: monoisopropylphosphoryl for DFP; singly aged *N*-monoisopropylphosphoroamidoyl and doubly aged H_2PO_3 for MIP. Observed *m/z* and Δ*m* values were not different from corresponding theoretical values ($p > 0.1$).

[c] No peak corresponding to a singly aged adduct of MIP was detected.

[d] The peak corresponding to the doubly aged active site peptide was confirmed by immunoprecipitation by a phosphopeptide antibody followed by SELDI-TOF-MS to obtain a single peak with the expected *m/z* value in the mass spectrum.

Table 5. Differences in average mass of MH^+ ions of active site peptides from intact or aged adducts of BChE with DFP or MIP [a,b]

Data type	Δ*m* DFP intact	Δ*m* DFP aged	Δ*m* MIP intact	Δ*m* MIP aged
Observed	165.0 ± 0.5	123.4 ± 0.7	162.9 ± 0.4	122.4 ± 0.7
Theoretical	164.1	122.1	162.2	121.1

[a] Data from Kropp and Richardson (2007).

[b] Values are means ± SEM ($n \geq 10$ experiments). The *m/z* values (average mass) for the MH^+ ion of the unreacted tryptic digest peptide containing the active site Ser are 2200.5 ± 0.1 (observed) and 2200.5 (theoretical). Theoretical values of Δ*m* (*m/z*) take into account the average mass of the Ser hydroxyl proton that is lost in the organophosphorylation reaction. Theoretical nonaged (intact) adducts for DFP and MIP are diisopropylphosphoryl and *N,N′*-diisopropylphosphoroamidoyl, respectively. Theoretical aged adducts for DFP and MIP are monoisopropylphosphoryl and *N*-monoisopropylphosphoroamidoyl, respectively. Observed *m/z* values were not different from corresponding theoretical values ($p > 0.1$).

Table 6. Differences in average mass of MH^+ ions of active site peptides from intact or aged adducts of NEST with DFP or MIP [a,b]

Data type	Δ*m* DFP intact	Δ*m* DFP aged	Δ*m* MIP intact	Δ*m* MIP aged[c]
Observed	ND[d]	123.0 ± 0.6	162.9 ± 0.4	162.9 ± 0.4
Theoretical	164.1	122.1	162.2	162.2

[a] Data from Kropp *et al*. (2004); theoretical values corrected by subtracting the average mass for H (1.01 Da).

[b] Values are means ± SEM ($n \geq 11$ experiments). The *m/z* values (average mass) for the MH^+ ion of the unreacted tryptic digest peptide containing the active site Ser are 2922.0 ± 0.2 (observed) and 2922.3 (theoretical). Theoretical values of Δ*m* (*m/z*) take into account the average mass of the Ser hydroxyl proton that is lost in the organophosphorylation reaction. Theoretical nonaged adducts for DFP and MIP are diisopropylphosphoryl and diisopropylphosphoroamidoyl, respectively. Theoretical aged adducts for DFP and MIP are monoisopropylphosphoryl and *N*-monoisopropylphosphoroamidoyl, respectively. Observed *m/z* values were not different from corresponding theoretical values ($p > 0.1$).

[c] No peak corresponding to a classically aged MIP adduct Δ*m* (+121.1 *m/v*) was detected. Only a peak corresponding to an intact MIP-NEST adduct was detected in kinetically aged (nonreactivatable) MIP-NEST, consistent with aged MIP-NEST being the deprotonated species, which would be protonated under the acidic conditions used for SELDI-TOF MS.

[d] No peak corresponding to a nonaged DFP adduct was detected, consistent with relatively rapid aging of the DPF-NEST conjugate (half-time of aging, 6.4 min).

Table 4 shows that DFP-inhibited AChE aged in the expected manner to give a peak in the SELDI-TOF MS spectrum corresponding to a monoisopropylphosphoryl adduct on the active site Ser peptide. However, no peak corresponding to a *N*-monoisopropylphosphoroamidoyl adduct on the active site peptide was detected in samples from kinetically aged MIP-inhibited AChE. Instead, a peak corresponding to a simple phosphate adduct (H_2PO_3) was detected. This surprising result was confirmed by immunoprecipitation using a phosphopeptide antibody followed by SELDI-TOF MS. The resulting spectrum consisted of a single peak corresponding to the active site peptide with a phosphate (H_2PO_3) adduct (bracketed by two peaks from internal molecular weight standards that were added to the MS chip). Thus, MIP-inhibited AChE ages by loss of both isopropylamine groups, as depicted in Fig. 1.

BChE inhibited by DFP or MIP aged in the conventional manner as shown by the MS data in Table 5. In each case, the mass spectra of kinetically aged samples showed disappearance of the peak corresponding to the intact OP adduct and appearance of a peak corresponding to the monoisopropylphosphyl adduct.

Aging of DFP-inhibited NEST resulted in a peak corresponding to the expected monoisopropylphosphoryl adduct, whereas the mass spectrum of kinetically aged MIP-inhibited NEST showed only the intact adduct. This result, coupled with the kinetics results showing complete aging at pH 8.0 and complete reactivation at pH 5.2 indicate that aging of MIP-inhibited NEST occurs by deprotonation of the acidic phosphoroamido hydrogen.

The different aging pathways for MIP-inhibited esterases are shown below in Fig. 1. It is noteworthy that the three MIP-inhibited esterases underwent aging by three distinct mechanisms (the details of which require further elucidation) to yield three different adducts. These results indicate that further research is needed to understand more fully the mechanisms of aging of phosphoroamidated serine esterases. In

addition, the fact that phosphoroamidates can inhibit esterases to yield different adducts has important implications for the delineation of biomarkers of exposure to OP compounds.

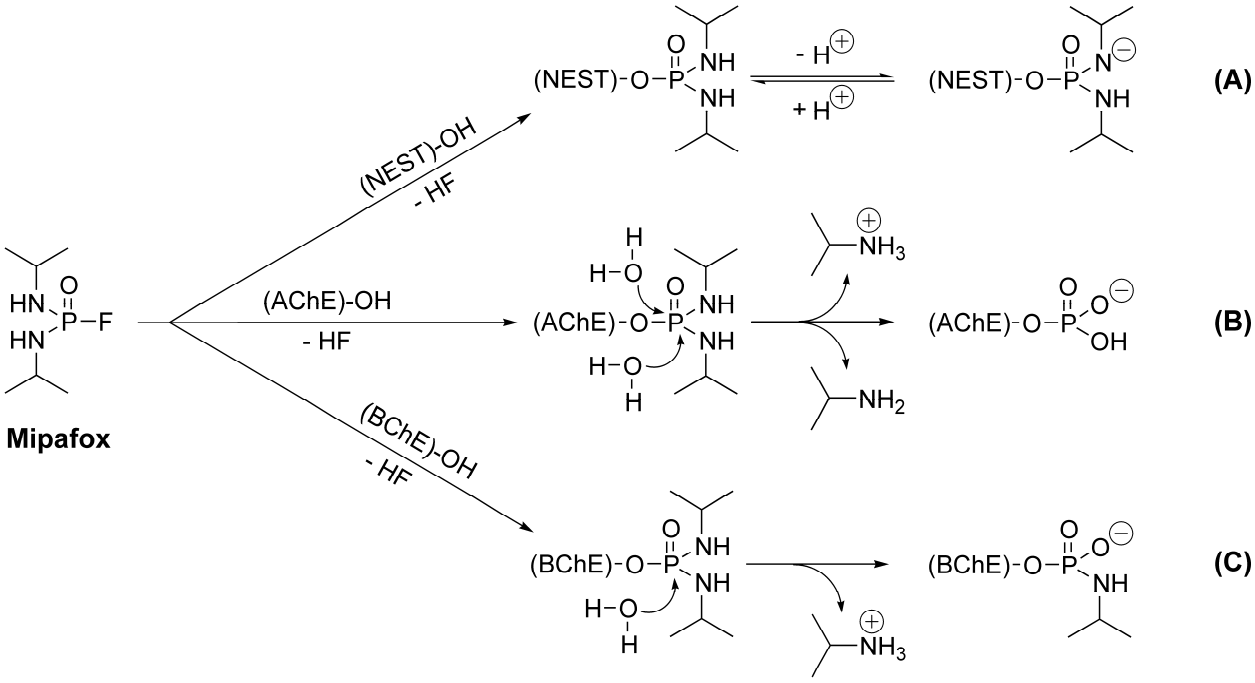

Figure 1. Pathways of inhibition and aging of MIP for three serine esterases. (A) NEST, (B) AChE, and (C) BChE. Inhibition of each serine hydrolase occurs by nucleophilic attack of the Ser hydroxyl on the phosphorus of MIP, displacing the primary leaving group, fluoride, and yielding an *N*,*N*′-diisopropyl-phosphorodiamido adduct, which then undergoes aging by a different mechanism for each enzyme. Although the exact mechanisms (S_N1 or S_N2) of aging for MIP-inhibited AChE and BChE require definitive elucidation, results to date are consistent with dual (AChE) or single (BChE) S_N2 displacement of isopropylamine by water as shown here. The charge of each aged moiety is shown as expected for pH 8.0, although these species would be expected to be protonated under the acidic conditions used for SELDI-TOF MS. (Reproduced from Kropp and Richardson, 2007).

5.3. *Computational molecular modeling*.

5.3.1. *Docking studies of isomalathion stereoisomers and Torpedo AChE*. Early computational molecular modeling work was carried out to investigate stereoselective inhibition of Torpedo AChE and other serine esterases by isomalathion stereoisomers as illustrated in Fig. 2. The results of computational docking studies were consistent with the experimental results obtained from kinetics and SELDI-TOF MS. Namely, that diethyl thiosuccinyl was the leaving group for (1*R*)-isomers and thiomethyl was the leaving group for (1*S*)-isomers of isomalathion (Doorn *et al*., 2003)

5.3.2. *Homology model of the patatin domain of NTE*. The three-dimensional structure of NTE is unknown. However, bioinformatics studies revealed that the catalytic (esterase) domain had sequence homology to patatin17 (pat17), a lipase found in potatoes and other plants whose crystal structure had been determined (Rydel *et al*., 2003). Using the structure of pat17 as a template, we constructed a homology model of the esterase domain of NTE (PNTE) as shown in Fig. 3 (Wijeyesakere *et al*., 2007; Wijeyesakere, 2009).

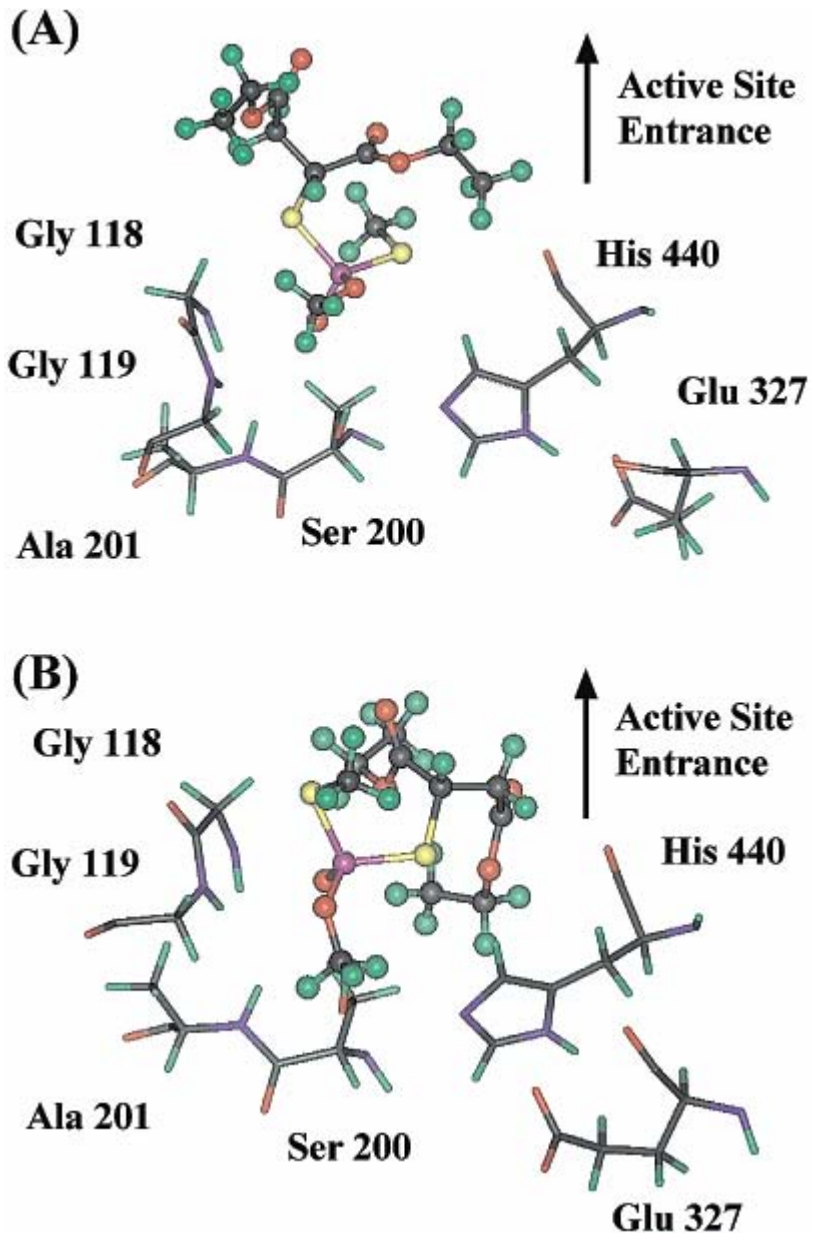

Figure 2. Results of computer-based docking experiments for isomalathion enantiomers and Torpedo AChE. (A) (1*R*,3*R*)- and (B) (1*S*,3*S*)-isomalathion in the active site of Torpedo AChE. The isomalathion enantiomers are in ball-and-stick format, whereas Torpedo AChE residues are displayed as sticks. Colors were assigned to atoms as follows: C, gray; H, green; N, blue; O, red; P, purple; and S, yellow. Only the catalytic triad and active site residues in close proximity to isomalathion are shown. The catalytic Ser 200 is located directly beneath the isomalathion phosphorus atom. Diethyl thiosuccinyl is predicted to be positioned apically to the active site Ser 200 for (1*R*,3*R*)-isomalathion. In contrast, thiomethyl is predicted to be positioned apically to Ser 200 for the (1*S*,3*S*)-enantiomer. The active site entrance is located directly above the isomalathion molecule in each panel as indicated by the arrow (Reproduced from Doorn *et al.*, 2003).

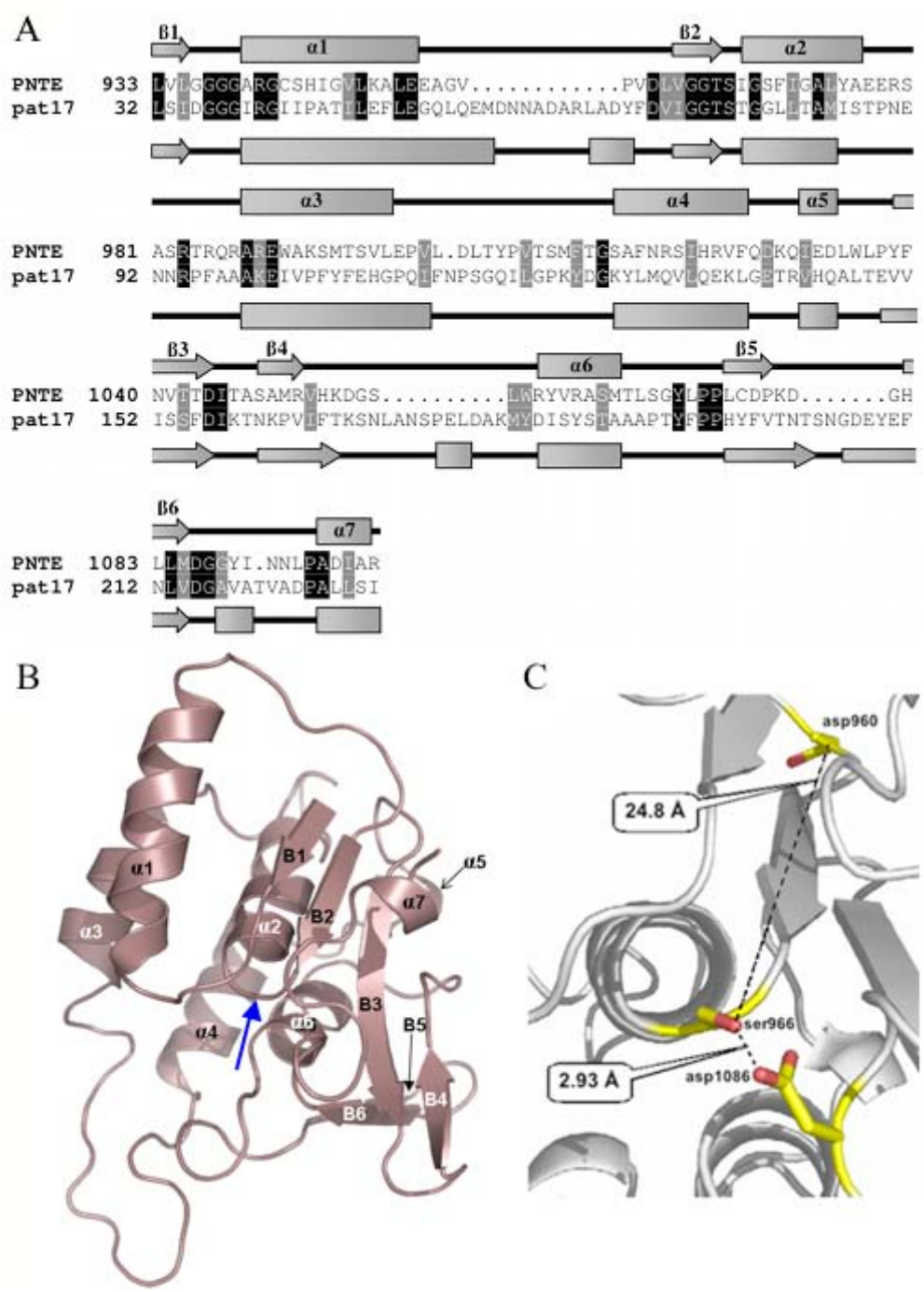

Figure 3. (A) Sequence alignment of PNTE and pat17. Identical residues are boxed in black; homologous residues in grey. Secondary structures of PNTE and pat17 are shown along with their respective primary structures as arrows (β-strands) and rectangles (α-helices). α-helices and β-strands in the PNTE sequence are numbered α1–α7 and B1–B6, respectively. (B) Ribbon diagram of the putative tertiary structure for PNTE. Blue arrow denotes the location of the nucleophilic elbow. (C) Organization of the predicted active site of PNTE, showing the proposed Ser966-Asp1086 catalytic dyad. Ser966, Asp960, and Asp1086 are depicted as capped sticks. Ser966 Oγ–Asp960 and Oδ2 Ser966 Oγ–Asp 1086 Oδ2 distances are shown as dotted lines. (Reproduced from Wijeyesakere *et al.*, 2007 with corrections in the sequence numbering from Wijeyesakere, 2009).

A major finding from the homology model of PNTE was that the active site was predicted to be a Ser966-Asp1086 catalytic dyad characteristic of certain lipases (Wijeyesakere *et al*., 2007) rather than the previously proposed Ser966-Asp960-Asp1086 catalytic triad (Atkins and Glynn, 2000).

5.3.3 *Docking, simulated inhibition, and simulated aging using the PNTE model*.

Docking studies were undertaken with DFP and MIP, using the PNTE model as the target. The structures of DFP and MIP were generated in Chem3D (CambridgeSoft, Cambridge, MA) and minimized using the MM2 protocol to a root mean square deviation (RMSD) gradient of 0.01 prior to their use in docking. Docking of DFP into the active site of PNTE was undertaken using the automated docking algorithm in Fujitsu CAChe (Fujitsu BioSciences, Sunnyvale, CA) employing a potential-mean-force technique with a Lamarckian genetic algorithm (run over 3,000 generations with a population size = 50, crossover rate = 0.8 and mutation rate = 0.3) (Morris *et al*., 1998). Flexibility was permitted in the ligands. The resulting models were analyzed in CAChe and PyMol (DeLano, 2002). Similar techniques were undertaken to dock MIP into the active site of PNTE in order to compare its binding affinity to that of DFP. This technique was similar to that carried out in our laboratory on other serine hydrolases and stereoisomers of isomalathion (although in those cases flexibility was allowed in both the ligand and a region of the macromolecule) (Doorn *et al*., 2001, 2003).

As shown in Fig. 4, Docking of DFP and MIP into the active site of PNTE revealed that the phosphorus atom of DFP was located 4.7 Å from Ser966 OG and 3.7 Å from Asp1086 OD2, while the phosphorus atom of MIP was located 5.2 Å from Ser966 OG and 4.2 Å from Asp1086 OD2. These results indicated that these OP compounds could be accommodated in the active site of the PNTE model in an orientation suitable for organophosphorylation. Moreover, the binding energies of DFP and MIP to the active site of PNTE were calculated to be -36.1 kcal/mol and -30.77 kcal/mol, respectively, thereby indicating favorable energetics for interactions between these ligands and the active site of PNTE (Wijeyesakere, 2009).

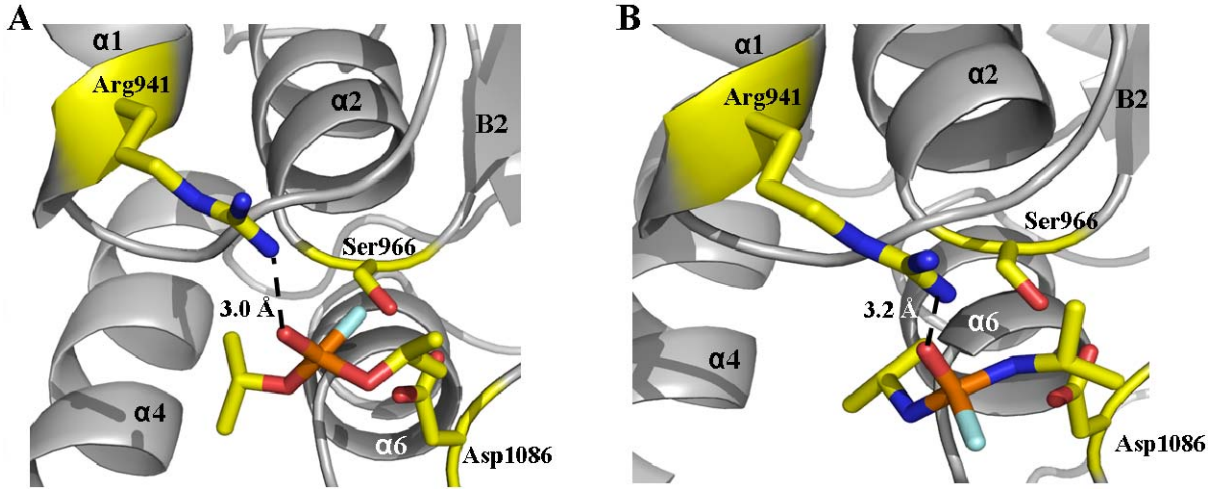

Figure 4. Docking DFP and MIP into the PNTE model. Docking of (A) DFP and (B) MIP into the active site of PNTE. The phosphoryl oxygens of the OP compounds make polar contact with Arg941 in the oxyanion hole with the Arg941 NH1 being 3.0 Å and 3.2 Å from the phosphoryl oxygens of DFP and MIP, respectively. (Reproduced from Wijeyesakere, 2009).

Analysis of the primary sequence of PNTE had previously indicated that Arg941 would be a potential candidate residue in the oxyanion hole formed by Gly938, Gly939, Ala940, and Arg941 (Wijeyesakere *et al*., 2007). Indeed, the results of the docking studies revealed that the NH1 of Arg941was located 3.0 Å

and 3.2 Å from the phosphoryl oxygen of DFP and MIP, respectively (Fig. 4). These results lend support to a role of Arg941 in the PNTE oxyanion hole and suggest that this residue stabilizes the OP ligand as it enters the PNTE active site in preparation for nucleophilic attack on the OP phosphorus by the Ser966 OG (Wijeyesakere, 2009).

Simulated inhibition and simulated aging studies were undertaken with aged and non-aged DFP (MIP was excluded in this portion of the study due to its unusual mechanism of aging via deprotonation as opposed to the loss an alkyl side-chain (Kropp *et al*., 2004). This allowed for testing *in silico* the hypothesis that aging results in a conformational change in PNTE that is distinct from the conformational change induced solely by inhibition. A similar computational procedure has been carried out recently through virtual mutation of a serine to phosphoserine (Groban *et al*., 2006).

Simulated inhibition was undertaken using the structure of diisopropylphosphoryl-serine (DPSer) that was built from the structure of monoisopropylphosphoryl-serine (MPSer) downloaded from the Hetero-compound Information Centre (http://alpha2.bmc.uu.se/hicup/; Kleywegt and Jones, 1998) using Chem3D. Ser966 in PNTE was replaced with DPSer using O 10.1 (Jones *et al*., 1991). The lego-loop procedure in O was employed to fix chain breaks arising from this substitution. Hydrogens were added to the DPSer-PNTE model at pH 7.0 followed by 300 rounds of minimization in Fujitsu CAChe using the MM3 protocol. Simulated aging of DPSer-PNTE was undertaken by deleting an isopropyl group from DPSer, thereby adding a negative charge to the resulting MPSer adduct. The MPSer-PNTE structure was minimized in Fujitsu CAChe using the MM3 protocol as described for simulated inhibition. The resulting structures were analyzed in CAChe and PyMol. Packing of residues around the PNTE active site in the minimized DPSer-PNTE and MPSer-PNTE models was undertaken via visual assessment.

The crystallography and NMR system (CNS; Brunger *et al.*, 1998) ver 1.2 was utilized to calculate the root-mean square deviation (RMSD) between the Cα backbones of native PNTE and DPSer-PNTE as well as the RMSD between the backbones of native PNTE and MPSer-PNTE. The calculated RMSD values were employed as a measure of the degree of overall conformational change arising from SI and SA of NTE by a neuropathic OP.

Fig. 5A shows that simulated inhibition resulted in a predicted expansion around the active site of PNTE, with the distance between the Ser966 OG and Asp1086 OD2 increasing to 5.2 Å, compared to 2.9 Å in the native PNTE structure. Simulated aging of the covalently bound DFP adduct resulted in a slight additional expansion around the active site relative to the inhibited state with the Ser966 OG and Asp1086 OD2 located 5.5 Å apart (compared to the 2.9 Å distance seen in the native structure) (Fig. 5B). This rotamer change is predumably due to charge repulsion betweent the negatively charged MPSer moiety and the negatively charged aspartate.

The negatively charged oxygen in the aged DFP adduct makes polar contact with Arg941 NH1 (2.7 Å), Gly938 N (3.4 Å) and Gly939 N (2.8 Å), which form the oxyanion hole of PNTE (Fig. 6). Thus, it can be seen that the negative charge on the aged OP adduct is stabilized by the oxyanion hole in a manner similar to that seen in normal catalysis with a carboxylic acid ester tetrahedral intermediate. This is also similar to the manner in which the oxyanion hole of AChE aids in the stabilization of the aged DFP adduct in the crystal structure of AChE (PDB ID 2dfp).

It was evident that covalent binding of DFP to Ser966 residue did not result in any significant conformational change in the overall tertiary structure of PNTE (Fig. 7A). The calculated Cα backbone deviation of native PNTE versus its DFP-inhibited state was 1.4 Å. In addition, simulated aging of the inhibited PNTE structure did not show any significant conformational change relative to its native and inhibited states (Fig. 7B). The calculated backbone RMSD between native PNTE versus its aged state was 1.6 Å. The backbone Cα deviation between the inhibited and aged states of PNTE was 0.2 Å.

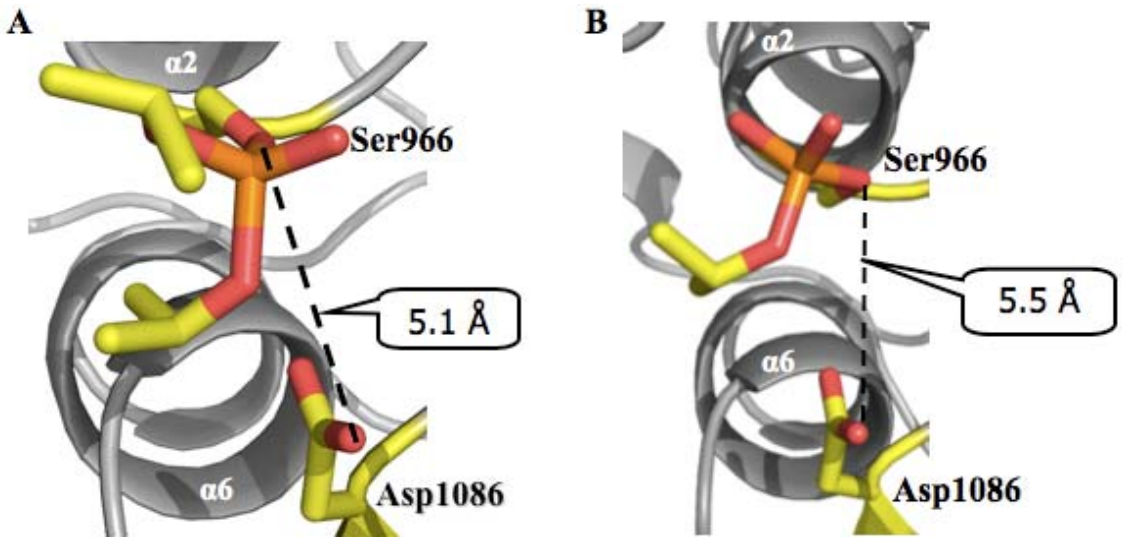

Figure 5. PNTE active site after simulated inhibition and simulated aging with DFP. (A). The model predicts that inhibition results in the active site Ser966 OG moving 5.1 Å away from Asp1086 OD2 (compared to 2.9 Å between these residues in the native PNTE structure). (B). Aging is predicted to result in a slight additional change, with the active site residues moving 5.5 Å apart (presumably due to charge repulsion by the negatively charged monoisopropylphosphoryl-Ser966 and Asp1086). However, these changes represent different rotamer conformations rather than perturbations in the amino acid backbones of these residues. (Reproduced from Wijeyesakere, 2009).

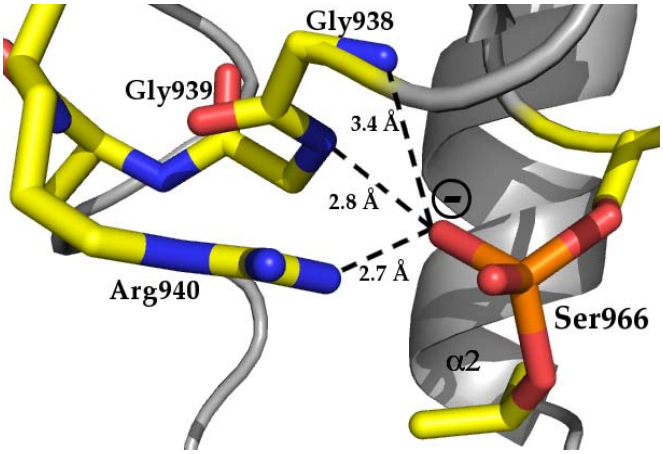

Figure 6. Simulated stabilization of the aged DFP-PNTE conjugate. The negative charge on the DFP-Ser966 adduct is stabilized by residues of the oxyanion hole (Gly938, Gly939 and Arg940), in a manner similar to what is expected for stabilization of the tetrahedral intermediate of an ester during normal catalysis and similar to that seen the crystal structures of other aged OP-serine esterase conjugates. The negatively charged oxygen is indicated along with contact distances between it and Gly938 N (3.4Å), Gly939 N (2.8 Å) and Arg940 NH1 (2.7 Å). (Reproduced from Wijeyesakere, 2009).

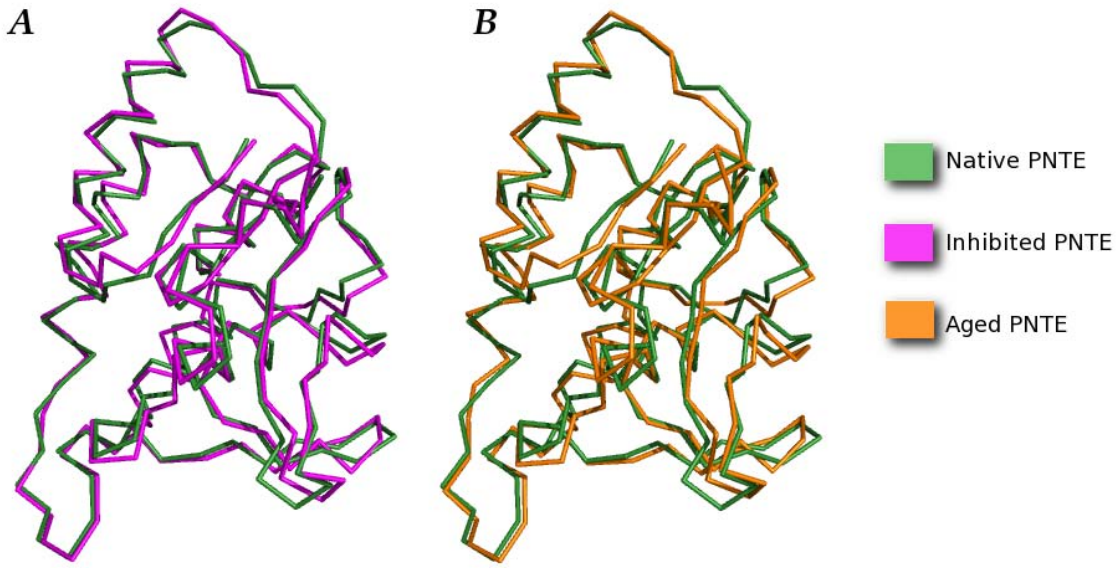

Figure 7. Simulated structural changes of PNTE Cα backbone after inhibition and aging. The Cα backbone structures of native PNTE (green) is compared to the backbone structures of PNTE following (A) inhibition by DFP (purple), or (B) aging of the DFP adduct (orange). Inhibition of PNTE does not result in a significant overall conformational change relative to its native state (Cα backbone RMSD = 1.4 Å). Similarly, aging is not associated with a significant conformational change relative to native PNTE (Cα backbone RMSD = 1.6 Å). (Reproduced from Wijeyesakere *et al*., 2009).

These findings can be compared to previous molecular dynamics research on AChE undertaken by Hurley *et al*. (2005) that reported a net-RMSD of 1.2 Å associated with *in silico* inhibition (but not aging) of AChE by the nerve agent VX. This RMSD is comparable to our result of 1.4 Å for simulated inhibition of PNTE by DFP. With respect to aging of an OP adduct, the X-ray crystal structures of *Torpedo californica* AChE inhibited and aged by DFP, sarin, and soman (PDB IDs 2dfp, 1cfj, and 1som, respectively) reported no significant conformational changes in the overall structure of the enzyme, although some localized conformational changes were reported in the AChE acyl pocket (Millard *et al*., 1999). Similarly, analysis of the crystal structure of native human BChE (PDB ID 1p0i) with its DFP- and echothiophate-aged forms (PDB ID 1xlu and 1xlv, respectively) shows no evidence for a global conformational change associated with aging (Nachon *et al*., 2005). The Cα RMSDs for the DFP- and echothiophate-aged forms of BChE relative to the native form of this enzyme are 0.51 Å (DFP-aged vs. native) and 0.55 Å (echothiophate-aged vs. native). This lack of a global conformational change following aging of an OP-esterase conjugate is consistent with the findings of our molecular modeling effort of the catalytic domain of NTE and serves to suggest that aging of NTE is not expected to result in a significant change in the structure of the enzyme relative to its native state.

Thus, if aging of NTE results in a toxic gain of function of the protein that is responsible for initiation of neurodegeneration (Glynn, 2000), then our modeling results on PNTE indicate that such a change does not arise from a global conformational change. On the other hand, initiation of neurodegeneration could arise from a loss of function of NTE, such as its proposed role in maintaining the homeostasis of membrane phospholipids (van Tienhoven *et al*., 2002; Vose *et al*., 2008; Zaccheo *et al*., 2004). Further research involving modeling and experimental studies on full-length NTE and related serine hydrolases will be required to address these important questions.

6. Bibliography (References)

Atkins, J., and Glynn, P. (2000). Membrane association and critical residues in the catalytic domain of human neuropathy target esterase. *J. Biol. Chem.* **275**, 24477-24483.

Brunger, A.T., Adams, P.D., Clore, G.M., DeLano, W.L., Gros, P., Grosse-Kunstleve, R.W., Jiang, J.S., Kuszewski, J., Nilges, M., Pannu, N.S., Read, R.J., Rice, L.M., Simonson, T., and Warren, G.L. (1998). Crystallography & NMR system: a new software suite for macromolecular structure determination. *Acta Crystallogr. D Biol. Crystallogr.* **54.** 905-921.

DeLano, W.L. (2002). *The PyMOL Molecular Graphics System*. DeLano Scientific LLC, San Carlos, CA, USA. http://www.pymol.org.

Doorn, J.A., Talley, T.T., Thompson, C.M., and Richardson, R.J. (2001). Probing the active sites of butyrylcholinesterase and cholesterol esterase with isomalathion: conserved stereoselective inactivation of serine hydrolases structurally related to acetylcholinesterase. *Chem. Res. Toxicol.* **14**, 807-813.

Doorn, J.A., Thompson, C.M., Christner, R.B., and Richardson, R.J. (2003). Stereoselective inactivation of Torpedo californica acetylcholinesterase by isomalathion: inhibitory reactions with (1R)- and (1S)-isomers proceed by different mechanisms. *Chem. Res. Toxicol.* **16**, 958-965.

Glynn, P. (2000). Neural development and neurodegeneration: two faces of neuropathy target esterase. *Prog. Neurobiol.* **61**, 61-74.

Groban, E.S., Narayanan, A., and Jacobson, M.P. (2006). Conformational changes in protein loops and helices induced by post-translational phosphorylation. *PLoS Comput. Biol.* **2**, e32.

Hurley, M.M., Balboa, A., Lushington, G.H., and Guo, J. (2005). Interactions of organophosphorus and related compounds with cholinesterases, a theoretical study. *Chem. Biol. Interact.* **157-158**, 321-325.

Jones, T.A., Zou, J-Y., Cowan, S.W., and Kjeldgaard, M. (1991). Improved methods for building protein models in electron density maps and the location of errors in these models. *Acta Crystallogr.* **A47**, 110-119.

Kleywegt, G.J., and Jones, T.A. (1998). Databases in protein crystallography. *Acta Crystallogr.* **D54**, 1119-1131.

Kropp, T.J., and Richardson, R.J. (2006). Aging of mipafox-inhibited human acetylcholinesterase proceeds by displacement of both isopropylamine groups to yield a phosphate adduct. *Chem. Res. Toxicol.* **19**, 334-339.

Kropp, T.J., and Richardson, R.J. (2007). Mechanism of aging of mipafox-inhibited butyrylcholinesterase. *Chem. Res. Toxicol.* **20**, 504-510.

Kropp, T.J., Glynn, P., and Richardson, R.J. (2004). The mipafox-inhibited catalytic domain of human neuropathy target esterase ages by reversible proton loss. *Biochemistry.* **43**, 3716-3722.

Millard, C.B., Kryger, G., Ordentlich, A., Greenblatt, H.M., Harel, M., Raves, M.L., Segall, Y., Barak, D., Shafferman, A., Silman, I., and Sussman, J.L. (1999). Crystal structures of aged phosphonylated acetylcholinesterase: nerve agent reaction products at the atomic level. *Biochemistry* **38**, 7032-7039.

Morris, G.M., Goodsell, D.S., Halliday, R.S., Huey, R., Hart, W.E., Belew, R.K., and Olson, A.J. (1998). Distributed automated docking of flexible ligands to proteins: parallel applications of AutoDock 2.4. *J. Comput. Chem*. **19**, 1639-1662.

Nachon, F., Asojo, O.A., Borgstahl, G.E., Masson, P., and Lockridge, O. (2005). Role of water in aging of human butyrylcholinesterase inhibited by echothiophate: the crystal structure suggests two alternative mechanisms of aging. *Biochemistry* **44**, 1154-1162.

Rydel, T.J., Williams, J.M., Krieger, E., Moshiri, F., Stallings, W.C., Brown, S.M., Pershing, J.C., Purcell, J.P., and Alibhai, M.F. (2003). The crystal structure, mutagenesis, and activity studies reveal that patatin is a lipid acyl hydrolase with a ser-asp catalytic dyad. *Biochemistry* **42**, 6696-6708.

van Tienhoven, M., Atkins, J., Li, Y., and Glynn, P. (2002). Human neuropathy target esterase catalyzes hydrolysis of membrane lipids. *J. Biol. Chem.* **277**, 20942-20948.

Vose, S. C., Fujioka, K., Gulevich, A. G., Lin, A. Y., Holland, N. T., and Casida, J. E. (2008). Cellular function of neuropathy target esterase in lysophosphatidylcholine action. *Toxicol. Appl. Pharmacol.* **232**, 376-383.

Wijeyesakere, S.J. (2009). Enzyme aging: structural insights from NTE and patatin. *PhD Dissertation*, The University of Michigan, Ann Arbor.

Wijeyesakere, S.J., Richardson, R.J., and Stuckey, J.A. (2007). Modeling the tertiary structure of the patatin domain of neuropathy target esterase. *Protein J.* **26**, 165-172.

Zaccheo, O., Dinsdale, D., Meacock, P.A., and Glynn, P. (2004). Neuropathy target esterase and its yeast homologue degrade phosphatidylcholine to glycerophosphocholine in living cells. *J. Biol. Chem.* **279**, 24024-24033.